Electronic Supplementary Material (ESI) for Materials Advances.

High photothermal conversion efficiency for semiconducting polymer/fullerene nanoparticles and its correlation with photoluminescence quenching

Supporting Information

Table of Contents

1. Photothemal Apparatus

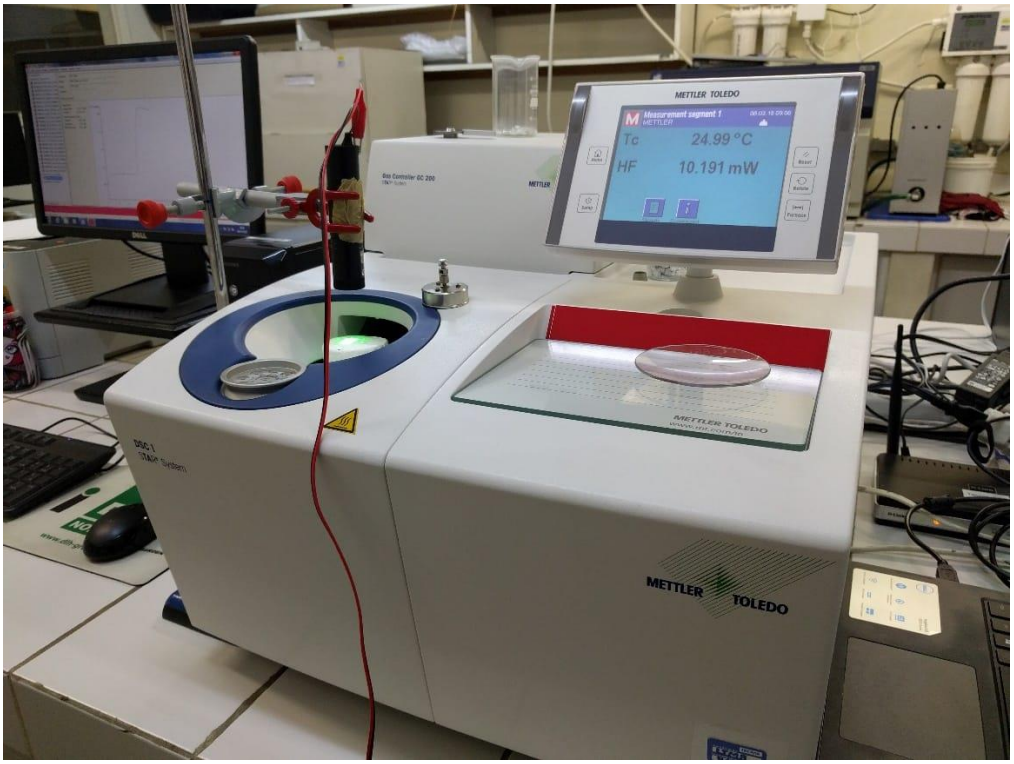

Figure S1. Photothermal experimental apparatus.

2. Histograms of nanoparticles sizes

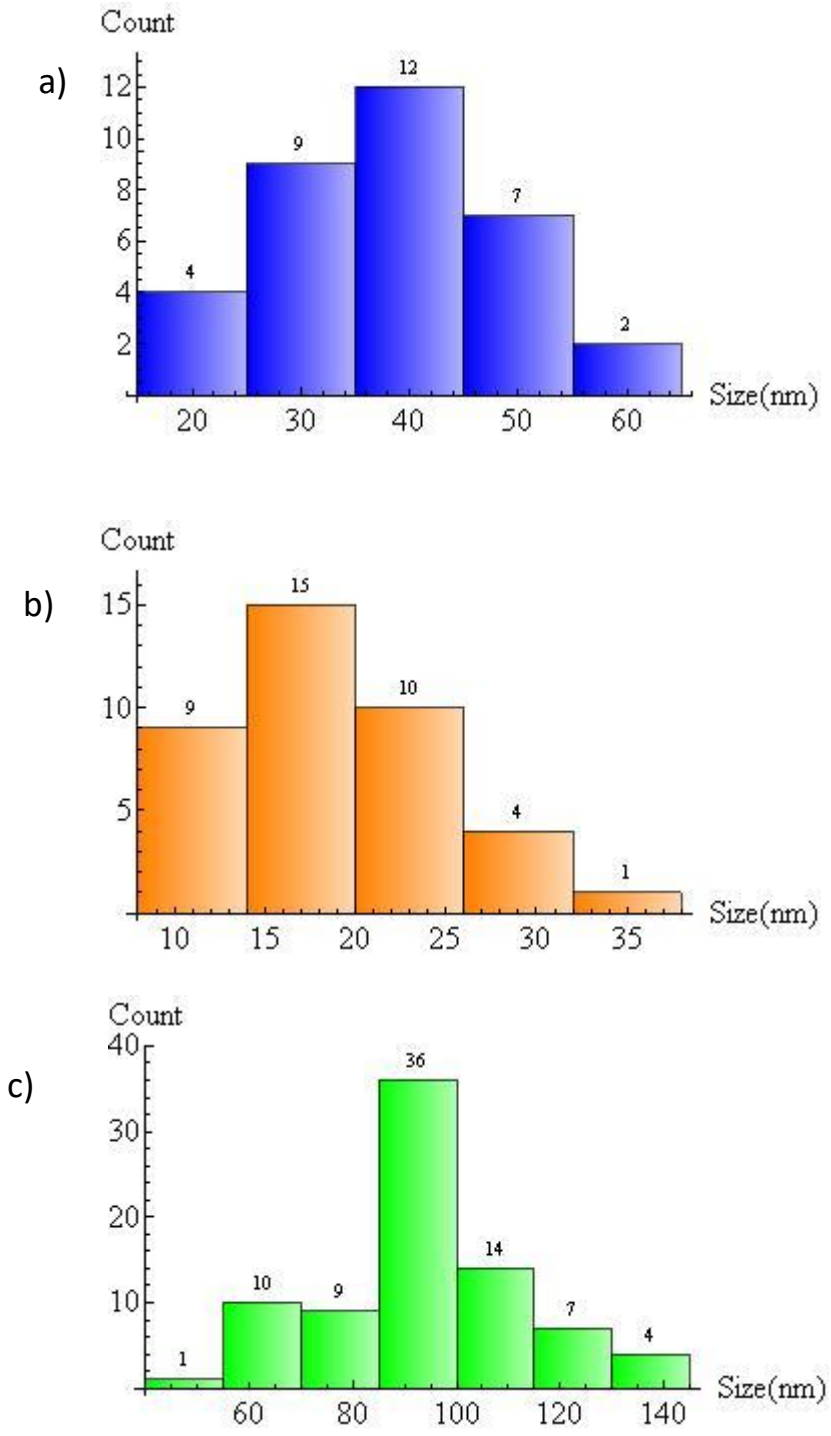

Figure S2. Histograms of polymer/fullerene nanoparticles sizes as obtained from a visual count using sections of TEM images. (a) P3HT/$PC_{71}BM$, (b) MDMO-PPV/$PC_{71}BM$, and (c) PSiF-DBT/$PC_{71}BM$. The numbers above each histogram corresponds to de number of the nanoparticles considered in the size interval.

3.UV-VIS measurements

3.1 UV-Vis Absorption Spectra of fullerene $PC_{71}BM$ nanoparticles

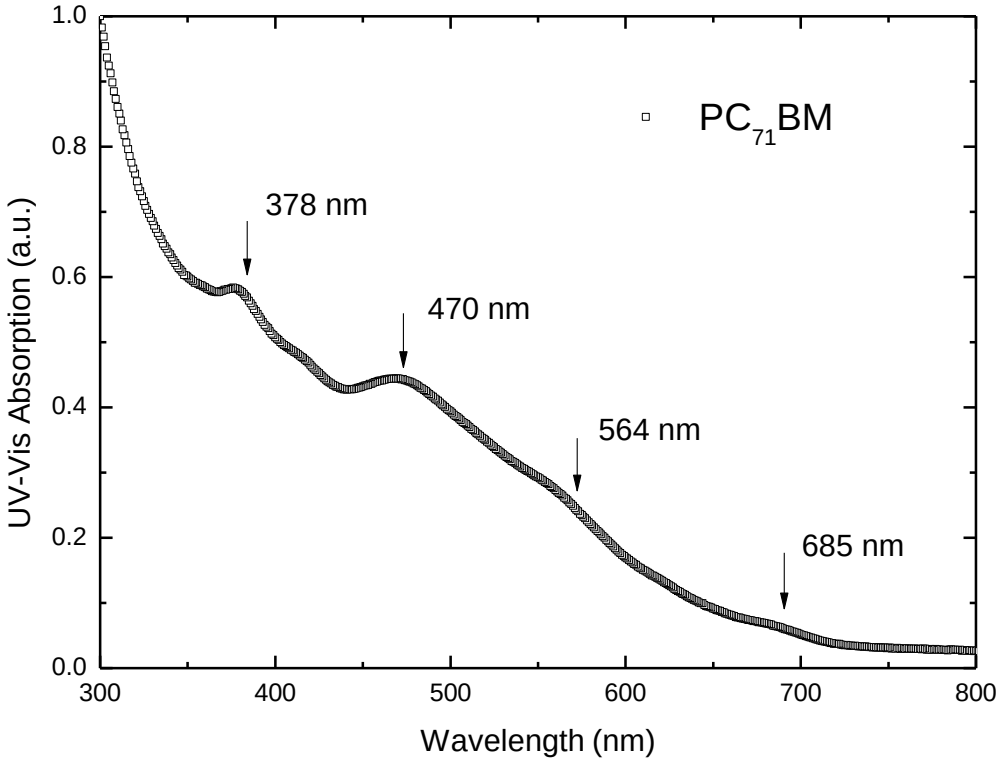

Figure S3. UV-Vis absorption spectra of pure $PC_{71}BM$ nanoparticles.

3.2 UV-Vis Absorption Spectra of polymers/$PC_{71}BM$ Heterojunction Nanoparticles

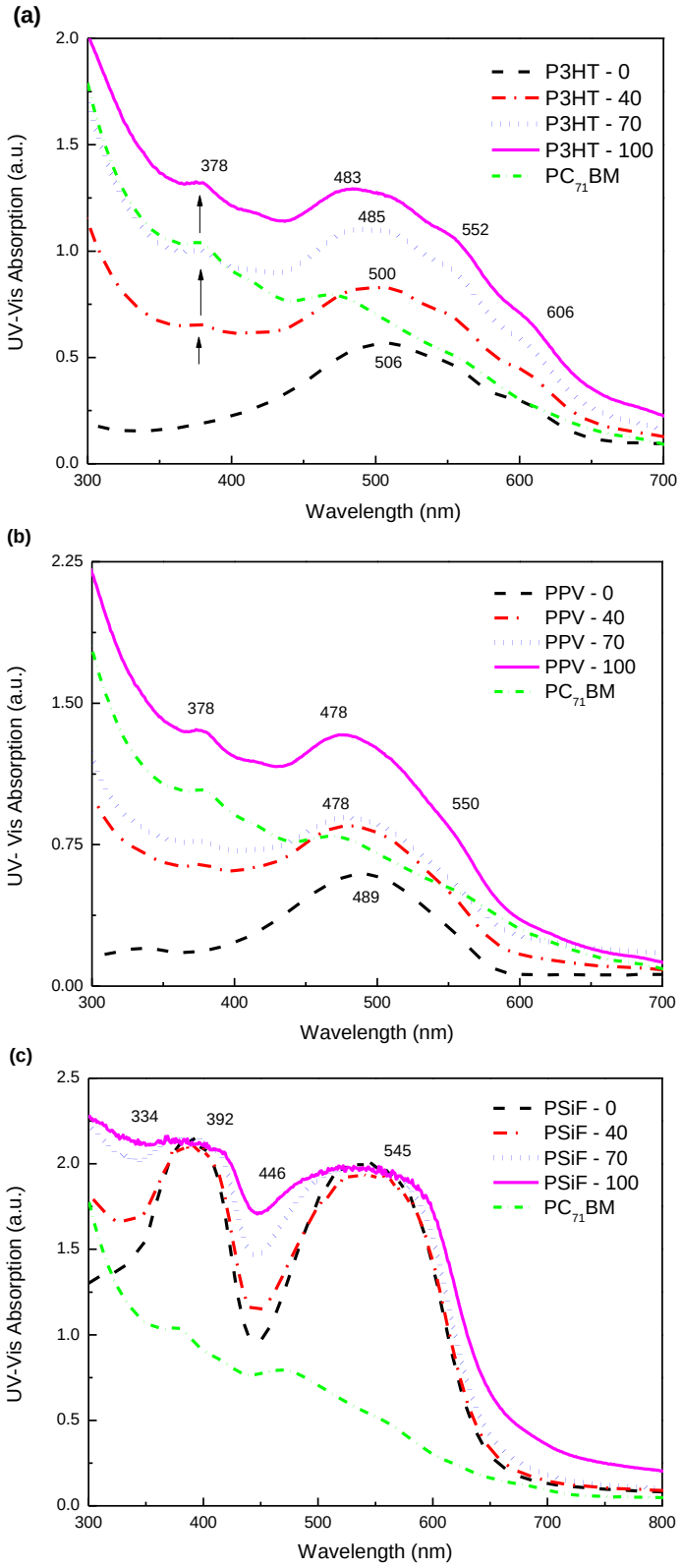

Figure S4. UV-Vis absorption spectra of (a) P3HT, (b) MDMO-PPV and (c) PSiF-DBT for pure conjugated polymer nanoparticles, pure fullerene $PC_{71}BM$ nanoparticles and polymer/$PC_{71}BM$ heterojunctions nanoparticles with fullerene doping amount of 40%, 70% and 100%. The inset in PL spectra shows the emission intensity for samples of fullerene doping amount of 40%, 70%, 100% and $PC_{71}BM$ nanoparticles.

4. Heat Capacity of Deionized Water

The average values for specific isobaric heat capacities of deionized water, with a relative standard deviation < 1%, at temperatures between 27.0 ºC and 38.0 ºC are presented in **Table S1**. Previous studies reported a specific heat capacity for liquid water 4.1826 J $ºC^{-1}$ g^{-1} at 25 ºC and 4.1855 J $ºC^{-1}$ g^{-1} at 35 ºC[1]. From the results obtained for deionized water it was possible to assure the viability of the Stepwise Method. It was then possible to proceed with experimental measurements for specific heat capacity of the nanoparticles.

Table S1. Specific heat capacity of deionized liquid water at heating rate 1 ºC min^{-1} in the temperature range of 27-38 ºC.

T (ºC)	C_p Liquid Water (J/ºC/g)	T (ºC)	C_p Liquid Water (J/ºC/g)
27.0	4.121	33.0	4.149
28.0	4.165	34.0	4.175
29.0	4.194	35.0	4.169
30.0	4.222	36.0	4.193
31.0	4.121	37.0	4.191
32.0	4.128	38.0	4.185

5. Specific Heat Capacity of the Nanoparticles

Table S2. Specific heat capacities of (a) P3HT, (b) MDMO-PPV and (c) PSiF-DBT nanoparticles of pure conjugated polymers (0%) and conjugated polymer: $PC_{71}BM$ heterojunctions nanoparticles in $PC_{71}BM$ doping amounts of 40%, 70% and 100%.

(a)

T (ºC)	C_p P3HT:$PC_{71}BM$ (J ºC^{-1} g^{-1})			
	0%	**40%**	**70%**	**100%**
27.0	3.918	3.871	3.491	3.171
28.0	3.954	3.827	3.523	3.445
29.0	3.944	3.826	3.542	3.134
30.0	3.920	3.824	3.535	3.126
31.0	3.869	3.831	3.416	3.024
32.0	3.875	3.798	3.449	3.009
33.0	3.852	3.793	3.463	3.999
34.0	3.832	3.796	3.458	3.004
35.0	3.819	3.808	3.409	3.043
36.0	3.828	3.821	3.373	3.033
37.0	3.817	3.837	3.381	3.043
38.0	3.795	3.819	3.387	3.060

(b)

T (ºC)	C_p MDMO-PPV:$PC_{71}BM$ (J ºC^{-1} g^{-1})			
	0%	**40%**	**70%**	**100%**
27.0	4. 062	3.799	3.457	2.866
28.0	4. 028	3.845	3.509	2.841
29.0	4.037	3.882	3.525	2.820
30.0	4.046	3.868	3.512	2.814
31.0	4.028	3.759	3.393	2.716
32.0	4.012	3.778	3.387	2.720
33.0	4.019	3.783	3.395	2.728
34.0	4.033	3.782	3.399	2.741
35.0	3.979	3.787	3.372	2.604
36.0	3.967	3.755	3.293	2.637
37.0	3.978	3.770	3.301	2.657
38.0	3.991	3.777	3.294	2.681

(c)

T (ºC)	C_p PSiF-DBT:$PC_{71}BM$ (J ºC^{-1} g^{-1})			
	0%	**40%**	**70%**	**100%**
27.0	4.763	3.899	3.604	2.289
28.0	4.425	3.964	3.665	2.906
29.0	4.473	4.000	3.672	2.944
30.0	4.504	4.039	3.675	2.958
31.0	4.350	3.973	3.638	2.736
32.0	4.369	3.973	3.578	2.979
33.0	4.365	4.008	3.589	2.808
34.0	4.358	3.999	3.592	2.775
35.0	4.330	3.979	3.552	2.649
36.0	4.311	3.945	3.522	2.676
37.0	4.314	3.961	3.535	2.699
38.0	4.305	3.965	3.537	2.730

In literature, specific heat capacity was reported for conjugated polymer P3HT, PPV derivatives and fullerenes[2-6]. Zhao J. *et al.* reported the phase diagram and specific heat capacity of thin films of P3HT/PCBM[7] and MDMO-PPV/PCBM[8] blends. Specific heat capacity of pure P3HT, MDMO-PPV, PCBM and blends P3HT/PCBM and MDMO-PPV/PCBM, in different PCBM weight fractions were measured by means of modulated temperature differential scanning calorimetry (MTDSC). In agreement with our work, they showed that specific heat capacity decreased as the PCBM weight fraction increases.

Table S3. Weight percentage (%) of fullerene in the nanoparticles used for photo-thermal measurements

Heterojunctions	Nanoparticles Mass (mg)			
	$PC_{71}BM$ weight percentage (%)			
	0	40	70	100
P3HT:$PC_{71}BM$	74.6	68.6	71	69.9
MDMO-PPV:$PC_{71}BM$	69.5	66.2	71.5	67
PSiF-DBT:$PC_{71}BM$	66.2	68.5	70.5	70.2

6. Equation for the Photo-thermal Conversion Efficiency (PCE)

The estimative of the photo-thermal efficiency was inspired in the method proposed by V. P. Pattani and J. W. Tunnell in Ref.[9]. Applying the energy balance during the laser illumination, the heat flux can be writes as

$$\frac{dH}{dt} = H_{in} - H_{out}\ , \tag{S1}$$

where H_{in} is the heat generated by the light absorption and H_{out} is the heat that escape from the sample.

H_{in} can be decomposed in two contributions: the heat produced by nanoparticles and the heat produced by the solvent (H_{sol}) so that

$$H_{in} = \eta(1 - 10^{-ABS})I + H_{sol}, \tag{S2}$$

where η is the PCE of the nanoparticles, I is the laser intensity, and ABS is the sample absorbance at the laser's wavelength (λ). Equation (S2) was written assuming that the solvent absorption at λ is negligible compared to the absorption of the nanoparticles so that H_{sol} can be considered a constant. Based on the Fourier's law we assume that

$$H_{out} = \alpha H, \tag{S3}$$

where α is a time constant related to thermal conductivity of the system and area of the sample[9]. Substituting Eqs. (S3) and (S2) in Eq. (S1) and solving the resulting differential equation one gets

$$H(t) = \eta(1 - 10^{-ABS})I\ (1 - e^{-\alpha t}) + H_{sol}\ . \tag{S4}$$

When the laser is switched off, the balance Eq. (S1) is

$$\frac{dH}{dt} = -H_{out} = -\alpha H\ . \tag{S5}$$

The solution of eq. (S5) is simple $(t) = H_0 e^{-\alpha t}$, where H_0 is the heat produced during the period of illumination. Hence from the decay of the heat flux observed just after switching the laser

off, it is possible to determine the time constant α. Using Eq. (S4) and taking $t = \Delta t$ as the total interval of laser irradiation, from Eq. (S4) one gets

$$\eta = \frac{H}{P_{laser}\Delta t\,(1-10^{-ABS})(1-e^{-\propto \Delta t})} - \frac{H_{sol}}{P_{laser}\Delta t\,(1-10^{-ABS})}, \tag{S6}$$

where $I = P_{laser}\Delta t$.

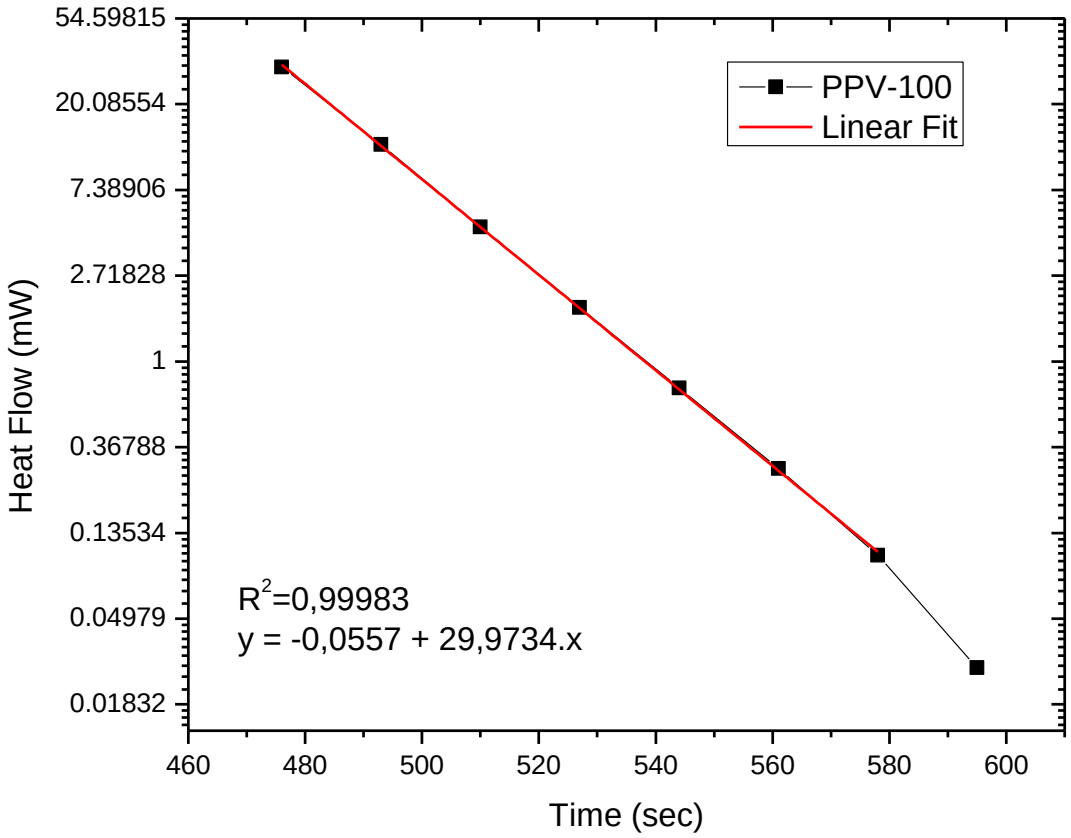

Figure S5. represents the linear fitting of eq. (S5) of 2nd minute of the PPV-100 nanoparticles photo-thermal measurement in the period of time when the laser is switched off to the thermal stability of sample (heat generated equal to 0mW).

7. Energy Levels and Characteristic Rates

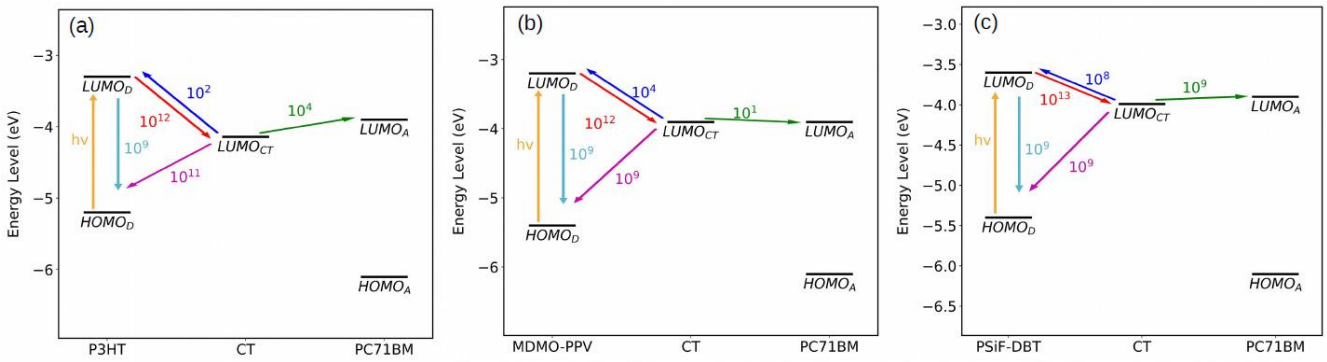

Figure S6. Energy levels diagram at the D/A heterojunction and magnitudes of calculated characteristic rates after donor photoexcitation as determined from the model described in section 3.1.

8. Voltage Loss in OSCs with Fullerene

Table S4. Open Circuit Voltages and Effective Gaps of some Organic Solar Cells reported in the literature.

Heterojunction Donor/Acceptor	No.	Ratio (D:A)	V_{oc} (mV)	$HOMO_D$ (eV)	$LUMO_A$ (eV)	$E_{g,eff}$ (eV)	Ref.
P3HT/ $PC_{61}BM$	**1**	1:1	0.60	-5.08	-4.38	0.7	10
	2	1:1	0.56	-4.58 ± 0.02	-	0.88	11
	3	1:1	0.58	-4.60 ± 0.01	-	0.90	11
	4	1:1	0.57	-4.61 ± 0.02	-	0.91	11
	5	1:1	0.61	-4.62 ± 0.02	-	0.92	11
	6	1:1	0.61	-4.66 ± 0.03	-	0.96	11
	7	1:1	0.49	-4.9	-3.8	1.1	12
	8	1:1	0.58 ± 0.02	-5.0	-3.74 ± 0.02	1.3	13
	9	1:1	0.77	-	-	1.3[a]	14
	10	1:0.8	0.60	-	-	1.5	15
	11	1:1	0.76 ± 0.03	-	-	1.5	16
	12	1:1	0.50	-	-	1.5	17
	13	1:1	0.45	-5.2	-3.7	1.5	18
	14	1:1	0.476	-5.2	-3.7	1.5	18
	15	1:1	0.503	-5.2	-3.7	1.5	18
	16	1:1	0.465	-5.2	-3.7	1.5	19
	17	1:1	0.555	-5.2	-3.7	1.5	19
	18	1:1	0.511	-5.2	-3.7	1.5	20
	19	1:1	0.522	-5.2	-3.7	1.5	20
	20	1:1	0.564	-5.2	-3.7	1.5	20
	21	1:1	0.61	-	-	1.5	21
	22	1:2	0.71	-	-	1.5	21
	23	1:3	0.80	-	-	1.5	21
	24	1:4	0.83	-	-	1.5	21
Mean Values	-	-	**0.593 ± 0.025**	**5.05 ± 0.02**	**3.73 ± 0.02**	**1.3**	-
MDMO-PPV/ $PC_{61}BM$	**25**	1:1	0.85	-5.2	-4.38	0.82	19
	26	1:4	0.80	-4.93	-	1.23	22
	27	1:4	0.78	-4.90	-	1.2	22
	28	1:4	0.84	-4.97	-	1.3	22
	29	1:1	0.824	-5.0	-3.75	1.3	19
	30	1:1	0.725	-5.0	-3.75	1.3	19
	31	19:1	0.97	-	-	1.4[a]	14
	32	9:1	0.91	-	-	1.4[a]	14
	33	1:1	0.88	-	-	1.4[a]	14
	34	1:4	0.83	-	-	1.4[a]	14
	35	1:4	0.85 ± 0.02	-5.3	-3.74 ± 0.02	1.56	13
	36	4:1	0.92 ± 0.02	-	-	1.7	16
	37	1:1	0.88 ± 0.01	-	-	1.7	16
	38	1:4	0.83 ± 0.02	-	-	1.7	16

	39	1:1	0.87	-	-	1.7	23
MDMO-PPV/ $PC_{61}BM$	**40**	1:2	0 .84	-	-	1.7	23
	41	1:3	0.82	-	-	1.7	23
	42	1:4	0.82	-	-	1.7	23
	44	1:6	0.78	-	-	1.7	23
	45	1:4	0.796	-	-	1.7	24
	46	1:4	0.802	-	-	1.7	24
	47	1:4	0.816	-	-	1.7	24
Mean Values	**-**	-	**0.838 ± 0.02**	**-5.3**	**-3.74 ± 0.02**	**1.5**	-
PSiF-DBT/$PC_{61}BM$	**48**	1:2	0.90	-5.4	-4.3	1.1	25
	49	1:2	0.81	-5.4	-4.3	1.1	25
	50	1:2	0.90	-5.39	-	1.7	26
	51	1:3	0.51	-	-	1.7	27
Mean Values	**-**	-	**0.78**	**-5.4**	**-4.0**	**1.4**	-

The values of *Voc*, $HOMO_D$, and $LUMO_A$ were taken from the references indicated in the last column. When the energy of those frontier orbitals were not available in the respective reference, the effective gap ($E_{g,eff}$) was calculated using the energies in **Fig. 1** of the text and assuming the LUMO of the $PC_{61}BM$ at -3.7 eV[28]. The D:A ratio in the third column is weight/weight.

The different values of *Voc* obtained from the same reference corresponds to distinct devices reported in the same work. Those variations of *Voc* might be related to the fabrication processes, devices' architecture, electrode's materials, organic solvents applied to deposit the active layer, and (or) molecular weight of the donor.

9. Biocompatibility evaluation

a. EXPERIMENTAL

Materials

Neutral red dye and sodium bicarbonate were purchased from Sigma-Aldrich (San Luis, EUA); high glucose Dulbecco's Modified Eagle Medium (DMEM) with or without phenol red, fetal bovine serum (FBS), penicillin, streptomycin, and trypsin/EDTA from Gibco/Thermo Fisher Scientific (Waltham, EUA); crystal violet dye and ethanol, from Merk (Darmstadt, Germany); and all plastic material for cell culture from Sarstedt (Nümbrecht, Germany). Ultrapure water (18.2 MΩ cm, Millipore) was used in the preparation of all solutions and in all washing steps.

Nanoparticles processing for biological assays

MDMO-PPV/$PC_{71}BM$ with 1:1 fullerene (w/w%) were used to all biological assays. Nanoparticle suspensions were centrifuged at 5,000 rpm for 15 minutes using Amicon® Ultra-15 Centrifugal Filter Units (Merck Millipore - which retain molecules/particles larger than 10 KDa) to remove excessive solvent. The nanoparticles were then dispersed again in distilled water, resulting in a concentrated suspension at 0.15 mg/ml of material. Finally, the solution was sterilized using a PVDF membrane filter with 0.22 µm pores.

Dispersions containing different concentrations of nanoparticles were prepared from serial dilutions (1:10 ratio[29]) in water, which was also used as vehicle control for all biological assays. The amount of dispersion added to cell culture medium accounted for 20% of the final volume, resulting in nanoparticles concentrations ranging from 3 ng/ml to 30 µg/ml.

Cell culture

Murine fibroblasts Balb/3T3 clone A31 (ATCC, CCL-163) and melanoma cells B16-F10 (BCRJ, 0046) were cultivated in high glucose DMEM, supplemented with 10% FBS, 0.25 µg/mL of penicillin/streptomycin, and 1.57 g/L of sodium bicarbonate. Cells were maintained in a humidified incubator at 37ºC and 5% CO_2 and subcultured upon reaching maximum confluence of 80%. Cell lines identity was monitored by their respective morphology, growth pattern, and pellet color since melanoma cells produce melanin pigments. Cells for experiments were used for no more than 5 passages.

Biocompatibility screening

Cells were seeded into 96-well plates at the following densities (cells/cm2): 2.08 x 10^4 Balb/3T3 (fibroblasts), and 5.21 x 10^2 B16-F10 (melanoma). Nanoparticles or vehicle control were added after 24 hours, and cells were cultivated in their presence for 72 hours. Cells viability was determined using neutral red assay[30], cells were incubated with 0.04 mg/mL neutral red solution for 2 hours, retained dye into cells was eluted using 50% ethanol and 1% glacial acetic acid in water, and absorbance was read at 540 nm wavelength. Cells density/proliferation was evaluated by crystal violet staining[31], cells were incubated with 0.25 mg/mL crystal violet solution for 20 minutes, the dye was eluted using 33% glacial acetic acid in water, and absorbance was read at 570 nm. For all colorimetric assays, absorbances were measured using an EpochTM Microplate Spectrophotometer (BioTek Instruments).

Statistics

At least 4 independent experiments were performed for biocompatibility screening. Either ROUT or Grubbs tests were applied to identify outliers. A threshold of 30% reduction in any of the studied biocompatibility parameters compared to control was considered as biologically significant cytotoxicity[32].

b. RESULTS AND DISCUSSION

Nanoparticles biocompatibility *in vitro*

To verify the nanoparticles potential to be applied as antitumor therapeutic tools, we investigated their biocompatibility with a tumor cell model (melanoma) and non-tumor cells (fibroblasts), which are tumor microenvironment and normal tissues main representatives[33-35]. Two biocompatibility indicator assays were used: crystal violet staining for cell density/proliferation, and neutral red uptake for cellular endomembranes viability. For that, cells were exposed to six nanoparticles concentrations (3 ng/ml to 30 µg/ml) or vehicle control (water) for 72 hours. A threshold of 30% reduction in any of the studied parameters compared to vehicle control (i.e., below the dashed green line in **Figure S7**) was considered as biologically significant cytotoxicity[32]. Results show that nanoparticles concentration of up to 30 µg/ml do not significantly interfere with cells density or viability, regardless of cell type (**Figure S7**). However, it is worth noticing that melanoma cells tended to be more sensitive to nanoparticles in a concentration-dependent manner, which should be deeper investigated in further studies.

Taken together these preliminary results show that these nanoparticles retain their light absorption profile in biological environments and are biocompatible specially to normal cells. These

results might guide their further biological application studies, possible with laser combination, to specific target tumor cells.

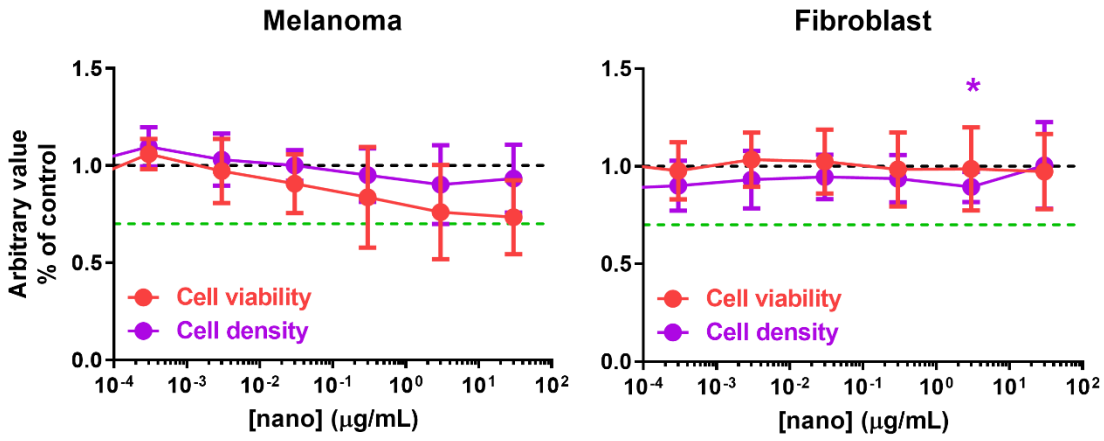

"Figure S7. Nanoparticles biocompatibility screening. Cells were cultivated in the presence of six nanoparticles concentrations or vehicle control (water) for 72 hours. Cells were colorimetric assayed for cell density determination (by crystal violet dye staining) and viability (by neutral red dye uptake). Results are shown as mean ± SD and represent at least four independent experiments performed in quadruplicate. All nanoparticle exposed groups were normalized by vehicle control (black dashed line, normalized as 1) of each respective experiment. Paired t test comparing each experimental group with the control. *, $p < 0.05$. Green dashed lines show the interval of 0-30% reduction of each parameter. [nano] = MDMO-PPV/PC71BM with 1:1 fullerene (w/w%) concentration"

10. References

1 D. C. Ginnings and G. T. Furukawa, Heat Capacity Standards for the Range 14 to 1200 degrees K. - correction, *J. Am. Chem. Soc.*, 1953, 75(24), 6359.

2 Z. Qian, L. Galuska, W. W. McNutt, M. U. Ocheje et al. Challenge and Solution of Characterizing Glass Transition Temperature for Conjugated Polymers by Differential Scanning Calorimetry, *J. Polym. Sci., Part B: Polym. Phys.*, 2019, 57, 1635-1644.

3 Y. Xu, X Wang, J. Zhou et al. Molecular engineered conjugated polymer with high thermal conductivity, *Sci. Adv.*, 2018, 4, eaar3031.

4 R. Dattani, J. H. Bannock, Z. Fei et al. A general mechanism for controlling thin film structures in all-conjugated block copolymer:fullerene blends, *J. Mater. Chem. A*, 2014, 2, 14711-14719.

5 J. Vandenbergh, B. Conings, S. Bertho, et al. Thermal Stability of Poly[2-methoxy-5-(20-phenylethoxy)-1,4-phenylenevinylene] (MPE-PPV):Fullerene Bulk Heterojunction Solar Cells, *Macromolecules*, 2011, 44(21), 8470-8478.

6 J. –H. Pohls, M. B. Johnson, M. A. White, Origins of Ultralow Thermal Conductivity in Bulk [6,6]-Phenyl-C61- Butyric Acid Methyl Ester (PCBM), *Phys. Chem. Chem. Phys.*, 2016, 18, 1185-1190.

7 J. Zhao, A. Swinnen, G. V. Assche, J. Manca, D. Vanderzande, B.V. Mele, Phase Diagram of P3HT/PCBM Blends and Its Implication for the Stability of Morphology, *J. Phys. Chem. B*, 2009, 113(6), 1587-1591.

8 J. Zhao, S. Bertho, J. Vandenbergh et al. Phase behavior of PCBM blends with different conjugated polymers, *Phys. Chem. Chem. Phys.*, 2011, 13, 12285-12292.

9 V. P. Pattani and J. W. Tunnel, Nanoparticle-Mediated Photothermal Therapy: A Comparative Study of Heating for Different Particle Types, *Lasers Surg. Med.*, 2012, 44(8), 675-684.

10 D. Veldman, S. C. J. Meskers, R. A. J. Janssen, The Energy of Charge-Transfer States in Electron Donor-Acceptor Blends: Insight into the Energy Losses in Organic Solar Cells, *Adv. Funct. Mater.*, 2009, 19, 1939-1948.

11 N. Chandrasekaran, A. Kumar, L. Thomsen, D. Kabra, C. R. McNeill, High performance as-cast P3HT:PCBM devices: understanding the role of molecular weight in high regioregularity P3HT, *Mater. Adv.*, 2021, 2, 2045-2054.

12 Y. Zhong, A. Tada, S. Izawa, K. Hashimoto, K. Tajima, Enhancement of V_{oc} without Loss of J_{SC} in Organic Solar Cells by Modification of Donor/Acceptor Interfaces, *Adv. Energy. Mater.*, 2013, 4, 1301332.

13 M. A. Faist, T. Kirchartz et al. Competition between the Charge Transfer State and the Singlet States of Donor or Acceptor Limiting the Efficiency in Polymer:Fullerene Solar Cells, *J. Am. Chem. Soc.*, 2012, 134, 685-692.

14 K. Vandewal, A. Gabisa et al. The Relation Between Open-Circuit Voltage and the Onset of Photocurrent Generation by Charge-Transfer Absorption in Polymer:Fullerene Bulk Heterojunction Solar Cells, *Adv. Funct. Mater.*, 2008, 18, 2064-2070.

15 W. Ma, C. Yang, X. Gong, K. Lee, A. J. Heeger, Thermally Stable, Efficient Polymer Solar Cells with Nanoscale Control of the Interpenetrating Network Morphology, *Adv. Funct. Mater.*, 2005, 15, 1617-1622.

16 K. Vandewal, K. Tvingstedt, A. Gabisa, O. Inganas, J. V. Manca, On the origin of the open-circuit voltage of polymer-fullerene solar cells, *Nature Mater.*, 2009, 8, 904-909.

17 D. Chen, A. Nakahara, D. Wei, D. Nordlund, T. P. Russel, P3HT/PCBM Bulk Heterojunction Organic Photovoltaics: Correlating Efficiency and Morphology, *Nano Lett.*, 2011, 11, 561-567.

18 S. Arora, S. K. Rajouria, P. Kumar, P. K. Bhatnagar, M. Arora, R. P. Tandon, Role of donor-acceptor domain formation and interface states in initial degradation of P3HT:PCBM-based solar cells, *Phys. Scr.*, 2011, 83, 035804.

19 M. Girtan and M. Rusu, Role of ITO and PEDOT:PSS in stability/degradation of polymer:fullerene bulk heterojunctions solar cells, *Solar Energy Materials & Solar Cells*, 2010, 94, 446-450.

20 L. Weimin, G. Jinchuan, S. Xiuquan, Z. Bin, Effect of solvents on the performance of P3HT:PCBM solar cells, *Optoelectronic Devices and Integration III*, 2010, 7847, 784709.

21 V. Shrotriya, J. Ouyang, R. J. Tseng, G. Li, Y. Yang, Absorption spectra modification in poly(3-hexylthiophene):methanofullerene blend thin films, *Chem. Phys. Lett.*, 2005, 411, 138-143.
22 A. Yaman, S. E. San, Y. Yerli, Efficiency Dependency of MDMO-PPV Based Polymer Solar Cells on Surface Morphology and Molecular Weight, *Mater. Sci.*, 2018, 5, 01-06.
23 H. Hoppe, M. Niggemann et al. Nanoscale Morphology of Conjugated Polymer/Fullerene-Based Bulk-Heterojunction Solar Cells, *Adv. Funct. Mater.*, 2004, 14(10), 1005-1011.
24 M. T. Rispens, A. Meetsma, R. Rittberger, C. J. Brabec, N. S. Sariciftci, J. C. Hummelen, Influence of the solvent on the crystal structure of PCBM and the efficiency of MDMO-PPV:PCBM 'plastic' solar cells, *Chem. Commun.*, 2003, 2116-2118.
25 X. Gong, Toward high performance inverted polymer solar cells, *Polymer*, 2012, 53, 5437-5448.
26 E. Wang, L. Wang, L. Lan, C. Luo, W. Zhuang et al. High-performance polymer heterojunction solar cells of a polysilafluorene derivative, *Appl. Phys. Lett.*, 2008, 92, 033307.
27 Y. Garcia-Basabe, C. F. N. Marchiori, B. G. A. L. Borges, N. A. D. Yamamoto, A. G. Macedo, M. Koehler, L. S. Roman, M. L. M. Rocco, Electronic structure, molecular orientation, charge transfer dynamics and solar cells performance in donor/acceptor copolymers and fullerene: Experimental and theoretical approaches, *Jour. Appl. Phys.*, 2014, 115, 134901.
28 Y. Kim, S. A. Choulis, J. Nelson, D. D. C. Bradley, S. Cook, J. R. J. Durrant, Composition and annealing effects in polythiophene/fullerene solar cells, *Mater. Sci.*, 2005, 40, 1371-1376.
29 ICCVAM-Recommended Test Method Protocol BALB/c 3T3 NRU Cytotoxicity Test Method, NIH Publication No. 07-4519, 2006.
30 G. Repetto, A. del Peso, J. L. Zurita, Neutral red uptake assay for the estimation of cell viability/cytotoxicity, *Nat Protoc.*, 2008, 3(7), 1125-1131.
31 R. J. Gillies, N. Didier, M. Denton, Determination of cell number in monolayer cultures, *Anal Biochem.*, 1986, 159(1), 109-113.
32 International Organization for Standardization, Biological evaluation of medical devices – Part 5: Tests for in vitro cytotoxicity, (ISO 10993-5:2009), (Switzerland, 2009).
33 F. Xing, J. Saidou, K. Watabe, Cancer associated fibroblasts (CAFs) in tumor microenvironment, *Front Biosci.* Review, 2010, 15(1), 166-179.
34 E. Marsh, D. G. Gonzalez, E. A. Lathrop, J. Boucher, V. Greco, Positional Stability and Membrane Occupancy Define Skin Fibroblast Homeostasis In Vivo, *Cell.*, 2018, 175(6), 1620-1633.e.13.
35 D. A. Yanez, R. K. Lacher, A. Vidyarthi, O. R. Colegio, The Role of Macrophages in Skin Homeostasis, *Pflugers Arch.*, 2017, 469(3-4), 455-463.